


## RESEARCH ARTICLE OPEN ACCESS

# Comparative Seasonal Trends and Potential Health Impacts of Arsenic and Chromium in Surface Water after Adsorption Using Highly Dispersed Fe<sub>3</sub>O<sub>4</sub> Nanoparticles

Tshimangadzo S. Munonde<sup>1</sup>  | Shirley K. Selahle<sup>2</sup><sup>1</sup>Institute for Nanotechnology and Water Sustainability, College of Science, Engineering and Technology, University of South Africa, Florida Science Campus, Roodepoort, South Africa | <sup>2</sup>Department of Chemistry, Faculty of Science, Engineering and Agriculture, University of Venda, Thohoyandou, South AfricaCorrespondence: Tshimangadzo S. Munonde ([munonts@unisa.ac.za](mailto:munonts@unisa.ac.za))

Received: 9 September 2024 | Revised: 9 November 2024 | Accepted: 14 November 2024

Keywords: arsenic | chromium | drinking water | physico-chemical properties | seasonal variation | water quality

## ABSTRACT

Surface water from springs, rivers, and dams is often used as an unconventional drinking water source in rural areas where potable water is often unavailable. However, this practice carries significant health risks due to potential contaminants. In this study, the concentrations of arsenic (As) and chromium (Cr) were assessed seasonally using graphite furnace atomic absorption spectrometry (GFAAS). Highly dispersed Fe<sub>3</sub>O<sub>4</sub> nanoparticles were synthesized, characterized, and utilized as adsorbents to remove As and Cr ions from various water matrices. The removal process was optimized by adjusting the mass of the nanoparticles, pH levels, and sonication time. To further understand the adsorption process, adsorption isotherms and kinetics were conducted. Physicochemical properties such as pH, electrical conductivity, and total dissolved solids were seasonally evaluated. The average As concentrations were in the range of 13.3–46.8 µg/L, while Cr was in the range of 1.02–5.04 µg/L. Expectedly, higher concentrations of As and Cr were observed in summer when there was intense precipitation, and the lowest concentrations were observed in winter, with little to no precipitation. The calibrated GFAAS displayed an excellent limit of detection, limit of quantification, and linearity of 0.092–0.13, 0.27–0.34, and 0.27–70 µg/L for As, while 0.031–0.07, 0.16–0.21, and 0.16–70 µg/L were attained for Cr, respectively. Arsenic levels exceeded 10 µg/L in all seasons, indicating that these concentrations were above the maximum permitted levels set by the World Health Organization and the South African National Standards. According to the health risk assessment, high As concentrations were alarming, as they were seasonally increasing, with the chronic daily intake exceeding the oral reference dose, whilst the incremental lifetime cancer risk was significantly high.

## 1 | Introduction

Water covers approximately 72% of the Earth's surface, yet it remains one of the most scarce resources, especially in developing countries [1, 2]. Access to clean water is essential for both urban and rural areas [3]. However, environmental pollution has significantly degraded surface and groundwater quality worldwide [4, 5]. Clean water is vital for human survival and is recognized

as a key factor in improving public health, as its availability helps prevent diseases and enhances sanitation, according to the World Health Organization (WHO) [6]. Alarming, more than 1 billion people across the globe still rely on untreated surface and groundwater, particularly in developing nations, where access to safe water is severely limited [5]. This crisis demands immediate attention and action to protect the most vulnerable populations and secure a healthier future.

This is an open access article under the terms of the [Creative Commons Attribution-NonCommercial-NoDerivs](https://creativecommons.org/licenses/by-nc-nd/4.0/) License, which permits use and distribution in any medium, provided the original work is properly cited, the use is non-commercial and no modifications or adaptations are made.

© 2024 The Author(s). *Analytical Science Advances* published by Wiley-VCH GmbH.

The contamination of water by trace metals is becoming a growing global environmental concern [7, 8]. Anthropogenic activities such as mining, wood preservation, and electroplating, amongst others, may cause the release of toxic substances into water bodies [9, 10]. Due to their bioaccumulation, non-degradability, and environmental persistence, researchers have conducted various research on toxic trace metals [11, 12]. The toxicity of some trace metals is relative as some of these trace metals are essential as micronutrients for the normal growth of humans and animals; however, they may also be toxic in excessive exposure [13]. Subsequently, metals such as arsenic (As), mercury, and lead may cause acute or chronic chemical toxicity and carcinogenicity even at their lowest concentrations [14, 15]. Trace metal contamination in water occurs through various pathways, negatively impacting both aquatic ecosystems and human health [16]. Therefore, studies focused on quantifying trace metals in water bodies are essential for assessing water quality and determining the level of contamination [17, 18], as this issue is increasingly becoming a worldwide environmental concern.

Thohoyandou and Makhado are situated in the south of the Vhembe district of the Limpopo province in South Africa [19]. These two towns are surrounded by numerous rural settlements situated on the outskirts of the built-up area [20, 21]. These two towns are largely populated, with over 1.2 million total population, and people depend on agricultural and industrial activities to sustain their living [22]. The industrial activities include wood preservation, sub-tropical agricultural farming, electroplating activities, and panel beating, amongst others [23]. These daily industrial activities increase the amount of waste produced, and some waste is discharged into rivers and dams [24].

In a study conducted by Edokpayi et al. [25], it was discovered that some sewage waste was being discharged into various rivers surrounding the two towns. However, most residents of the neighbouring villages come from disadvantaged backgrounds and rely on these rivers as their primary source of water for both domestic activities and drinking purposes [25, 26]. This exposes the villagers to various pollutants, including toxic trace metals such as As and chromium (Cr), amongst others [27]. Excessive exposure to toxic trace metals can lead to water-related health issues, including dysentery, diarrhoea, unintended pregnancy termination, premature birth, viral hepatitis, and gastric and duodenal ulcers [28, 29]. In the worst-case scenarios, As and Cr have been reported to cause harmful effects, including cellular damage, cancer development, and neurotoxicity in living organisms [30]. Due to these adverse effects, the maximum permitted levels for ingestion have been set at 10 µg/L for As and 50 µg/L for Cr [31, 32]. The WHO, alongside other water regulatory authorities, has adopted these standard limits, which are essential for maintaining water quality.

Nanomaterials, particularly magnetic Fe<sub>3</sub>O<sub>4</sub> nanoparticles, have been reported to facilitate the extraction and adsorption of trace metals in water due to their properties such as larger surface area, high selectivity, fast adsorption capability, and high efficiency [33]. Given their aggregation and agglomeration challenges, magnetic nanoparticles often require a protective coating to adsorb trace metals from water [34]. However, due to the advancements in synthesis methods, highly dispersed magnetic nanoparticles can be synthesized for use as adsorbents for the extraction

and removal of trace metals in water matrices [35, 36]. Thus, magnetic Fe<sub>3</sub>O<sub>4</sub> nanoparticles have attracted interest for use in the adsorption of trace metals due to their availability, cost-effectiveness, ready dispersibility in solutions, easy recovery, and fast adsorption kinetics [37, 38].

The purpose of this study was to characterize the water quality of selected rivers and dams in the Vhembe district by quantifying the concentrations of As and Cr in environmental water samples after adsorption using Fe<sub>3</sub>O<sub>4</sub> nanoparticles. The motivation for this study stems from the impact of various industrial activities in the area and the fact that many villagers consume river water without any form of treatment. This research was conducted with an emphasis on seasonal variations of both As and Cr. Additionally, key physicochemical properties, such as pH, electrical conductivity (EC), and total dissolved solids (TDS), were evaluated seasonally. The study also discussed other factors, including the influence of seasonal fluctuations in trace metal concentrations, potential sources that contribute to the increase of trace metals in surface water, and statistical analyses. Furthermore, the health impacts associated with elevated concentrations of As and Cr were assessed in this study.

## 2 | Study Area and Sample Collection

Thohoyandou and Makhado are two major towns in the Vhembe district, Limpopo Province, South Africa. The district is the center of attention for various industrial activities such as agricultural farming, wood preservation, and electroplating activities, amongst other activities. Additionally, various wastewater and drinking water treatment plants are located within the district's outskirts. Various major rivers flow across some of the regions where these activities occur. In this study, water samples were collected from various rivers, including Mvudi and Mutshundudi, located around Thohoyandou town. Then, sampling was further extended to the Luvuvhu River, which connects both Thohoyandou and Makhado. Sampling was also conducted at two dams, Albasin and Thathe, which are situated across the outskirts of Thohoyandou and Makhado towns and feed directly from Luvuvhu and Mutshundudi rivers, respectively. Both Mutshundudi and Luvuvhu rivers serve as a direct source of water not only for domestic activities but also for drinking purposes. The study area is shown in Figure 1.

Water samples from rivers and dams were collected through the Grab Sampling technique. Samples were collected in polyethylene bottles, washed with a detergent, and rinsed with deionized water and nitric acid to avoid external contamination. Before collecting the samples, 1 mL of 1% nitric acid was added to each sampling bottle to eliminate trace metal adsorption and hydrolysis. The collected samples were then stored in the refrigerator and analyzed within three days of collection. The first set of water samples was collected in the winter season (August). The second set of water samples was collected in the summer (September). The third set of water samples was also collected in summer (January); this was a rainy season, wherein most of the water sources were full to maximum capacity. The water samples were filtered through 0.22 µm filters (Sigma-Aldrich, St. Louis, MO, USA) and then analyzed in triplicates. Physiological properties such as pH, EC, and TDS were also measured in

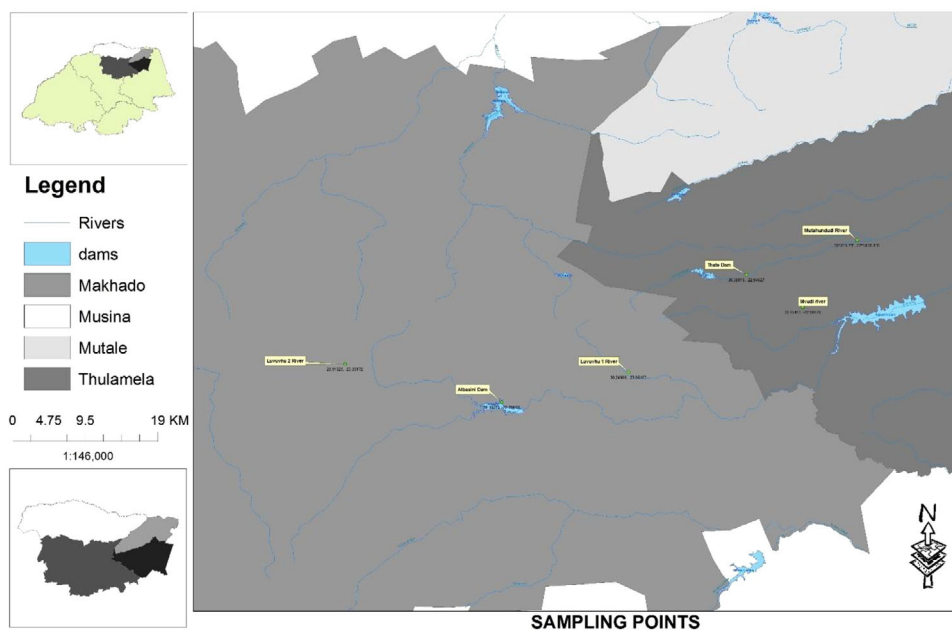


**FIGURE 1** | Map showing the sampling area alongside all the sampling points.

situ and monitored within the three collection times/seasons. For quality assurance (QA) and quality check (QC), drinking water CRMs (NIST 1643; Sigma-Aldrich, St. Louis, MO, USA) and procedure blank were analyzed after every 10 samples.

### 3 | Standards and Reagents

All solutions were prepared with high-purity (type 1) deionized water. Analytical-grade chemicals were used throughout the analysis. Before use, all glassware, wash bottles, and polyethylene bottles were washed with a detergent, soaked in 10%  $\text{HNO}_3$  solution (nitric acid [65%, v/v] was purchased from Sigma-Aldrich, St. Louis, MO, USA), and then rinsed three times with deionized water. As and Cr calibration sub-standards were purchased from Sigma-Aldrich (St. Louis, MO, USA). As and Cr calibration sub-standard solutions were prepared daily by serial dilutions from stock solutions of 1000 mg/L (Merck, Darmstadt, Germany) in deionized water and 10%  $\text{HNO}_3$ . A chemical matrix modifier used was a 100 mg/L Pd solution freshly prepared in ultra-pure deionized water from a 1000 mg/L standard solution (Merck, Darmstadt, Germany).

### 4 | Synthesis and Characterization of Magnetic $\text{Fe}_3\text{O}_4$ Nanoparticles

Magnetic  $\text{Fe}_3\text{O}_4$  nanoparticles were synthesized using a modified co-precipitation method previously published [32]. Practically, 5.1 g of  $\text{Fe}(\text{NO}_3)_3 \cdot 9\text{H}_2\text{O}$  (Sigma-Aldrich, St. Louis, MO, USA) and 2.5 g of  $\text{FeCl}_2 \cdot 4\text{H}_2\text{O}$  (Sigma-Aldrich, St. Louis, MO, USA) were dissolved in 100 mL of deionized water in an inert Argon atmosphere at 80°C, stirring at 7000 rpm for 20 min. To this solution, 25 mL of aqueous ammonia solution (25% v/v) (Sigma-Aldrich, St. Louis, MO, USA) was added into the solution to induce precipitation, leading to the solution changing from orange to black while forming black magnetic precipitates at the bottom of the flask

under stirring at 7000 rpm for 20 min. The formed magnetic  $\text{Fe}_3\text{O}_4$  nanoparticles were separated by magnetic decantation and washed several times with deionized water and ethanol before being dried in an oven at 100°C overnight. The particles were ground into a fine powder prior to their characterization.

The fine magnetic  $\text{Fe}_3\text{O}_4$  powder was characterized using the following: Fourier-transform infrared (FTIR) spectra were obtained on a PerkinElmer spectrum 100 FTIR spectrometer (Waltham, MA, USA). X-ray diffraction measurements were carried out on a Phillips P.W. 1710 X-ray powder diffractometer (Bruker AXS GmbH, Germany) with  $\text{Cu-K}\alpha$  radiation ( $\lambda = 0.1540$  nm, operating at 40 mA and 30 kV), PerkinElmer spectrum 100 FTIR spectrometer (Waltham, MA, USA). The morphology of the materials was determined using both transmission electron microscopy (TEM, JEM-2100; JEOL, Japan) and scanning electron microscopy (SEM, Auriga Cobra FIB FE-SEM, Germany) coupled with an energy dispersive X-ray spectroscopy (EDX).

### 5 | Instrumentation

A Varian SpectrAA 220 atomic absorption spectrophotometer equipped with a graphite tube atomizer (Varian GTA 110 series graphite furnace (Markham, ON, Canada), with a programmable sample dispenser linked to a signal processor-computer system was used for all analysis employing argon as a purging gas. The Thermo Scientific NESLAB ThermoFlex 900 Recirculating Chiller with Pump 1–115 V/60 Hz (Thermo Fisher Scientific, Waltham, Massachusetts, USA), which incorporates a highly reliable plumbing design, was used to eliminate leaks and improve performance on the GTA and to keep samples at the right temperature by supplying cooling water to the GTA. A new graphite tube (Agilent, South Africa) in which the samples were vaporized was used throughout the analysis. Hollow cathode lamps for As and Cr used in the analysis were from Photron

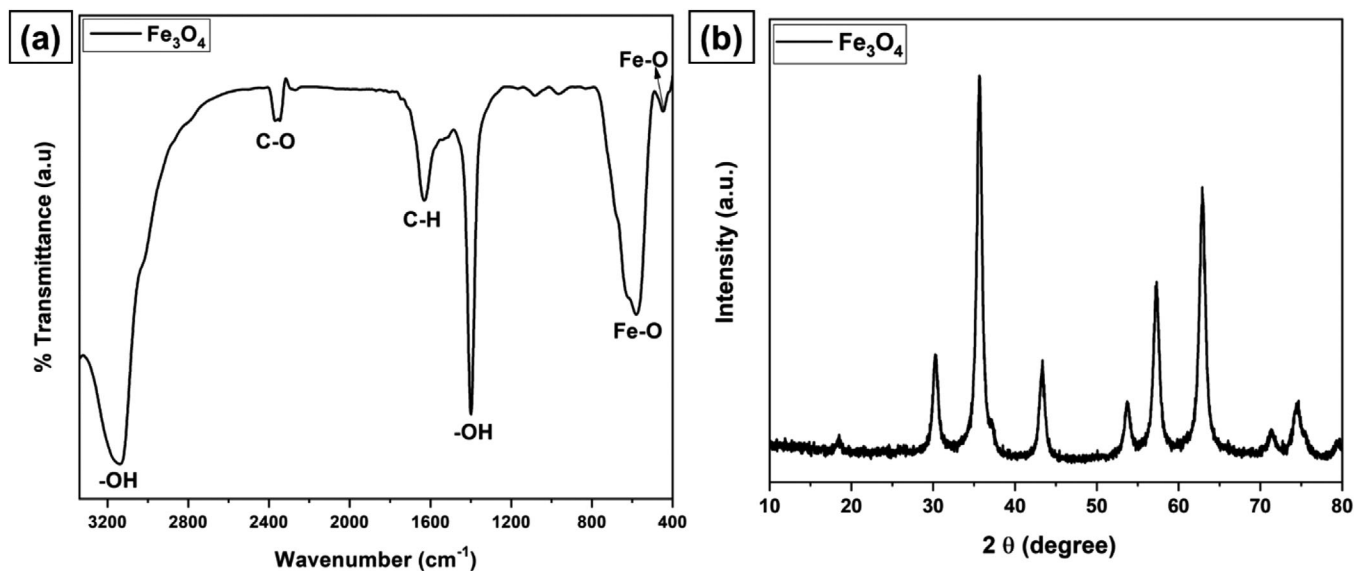


**FIGURE 2** | Fourier-transform infrared (FTIR) (a) and X-ray diffraction (XRD) (b) spectra of magnetic  $\text{Fe}_3\text{O}_4$  nanoparticles.

(Deblin Drive, Narre Warren, Victoria, Australia). The instrument was operated following the manufacturer's instructions. The Direct-Q 5 Ultrapure Water System manufactured by Merck, Darmstadt, Germany, was used to supply ultrapure type 1 water, which was used in the analysis. The pH and EC were measured on a WTW Multi 340i meter (Geotech Environmental Equipment, Inc., USA), with the pH meter calibrated using standard buffers of pH 4, 7, and 9 on a 3-point calibration. The EC measurements were done by immersing the probe in each sample and leaving the probe for 3 min to stabilize prior readings, with deionized water used to clean the probe after each reading. Similarly, the TDS readings were taken on an Extech EC 400 multimeter (Extech Instruments, Nashua, USA) following the EC measurement method.

## 6 | QA, QC, and Statistical Analyses

To ensure that QA and QC were observed, analytical reagents (Merck, Germany) grade chemicals and Milli-Q Millipore water were used to prepare all reagents and calibration standards. A chemical matrix modifier was used, and 100 mg/L Pd was prepared in ultra-pure deionized water. The sample blank and standard solutions were analyzed after every ten readings to calibrate the instrument. The relative standard deviation (RSD), mean, and standard deviations were calculated using MS Excel Office 365 (Microsoft Inc.).

## 7 | Results and Discussion

### 7.1 | Materials Characterization

#### 7.1.1 | FTIR and X-ray Diffraction Analysis

FTIR characterization was studied to gain insights into the molecular structure of the magnetic  $\text{Fe}_3\text{O}_4$  nanoparticles, as shown in Figure 2a. In the fingerprint region of the spectrum, it is possible

to visualize the two bands positioned at  $442\text{ cm}^{-1}$  and  $588\text{ cm}^{-1}$ , which are characteristics of the octahedral and tetrahedral Fe–O bond absorption, respectively. These highly pronounced bands confirm the presence of the magnetic core within the synthesized magnetic  $\text{Fe}_3\text{O}_4$  nanoparticles. The absorption band at  $3150\text{ cm}^{-1}$  represents water hydroxyls (OH) from the absorbed moisture. Similarly, the band around  $1405\text{ cm}^{-1}$  represents the OH stretching vibration of the absorbed water. The bands around  $1620\text{ cm}^{-1}$  represent the C–H group, whilst the band around  $2342\text{ cm}^{-1}$  can be ascribed to the C–O of the  $\text{CO}_2$  adsorbed from the atmosphere. The powder X-ray diffractograms Figure 2b displayed characteristics peaks at  $2\theta$   $18^\circ$ ,  $31^\circ$ ,  $35^\circ$ ,  $43^\circ$ ,  $54^\circ$ ,  $57^\circ$ ,  $64^\circ$ ,  $72^\circ$ ,  $75^\circ$  corresponding to the (220), (311), (400), (422), (511), and (440), which represent the inverse cubic spinel phase of  $\text{Fe}_3\text{O}_4$  (magnetite, JCPDS card no. 85-1436) [31]. The average particle size was predicted using the Debye Scherrer formula, calculated as 8 nm. The observed pattern and their corresponding particle size suggest the grafting of the pure inverse cubic spinel phase magnetic  $\text{Fe}_3\text{O}_4$  nanoparticles. Thus, the FTIR and X-ray diffraction (XRD) analysis confirm the successful synthesis of magnetic  $\text{Fe}_3\text{O}_4$  nanoparticles.

#### 7.1.2 | Field-emission scanning electron microscopy and transmission electron microscopy

The morphology of the magnetic  $\text{Fe}_3\text{O}_4$  nanoparticles was observed on field-emission scanning electron microscopy (FE-SEM) and transmission electron microscopy (TEM). Figure 3a shows that the highly dispersed and uniformly spherical  $\text{Fe}_3\text{O}_4$  nanoparticles were observed. The particle size of the observed nanoparticles ranged between 44 and 260 nm, with an average particle size of 93 nm. Notably, the nanoparticles were not highly agglomerated, which might have resulted from the high-speed stirring that was done before and after the formation of the nanoparticles. This is more apparent in the TEM image Figure 3b, which shows the well-dispersed nanoparticles. Due to less agglomeration of the nanoparticles, it is anticipated that



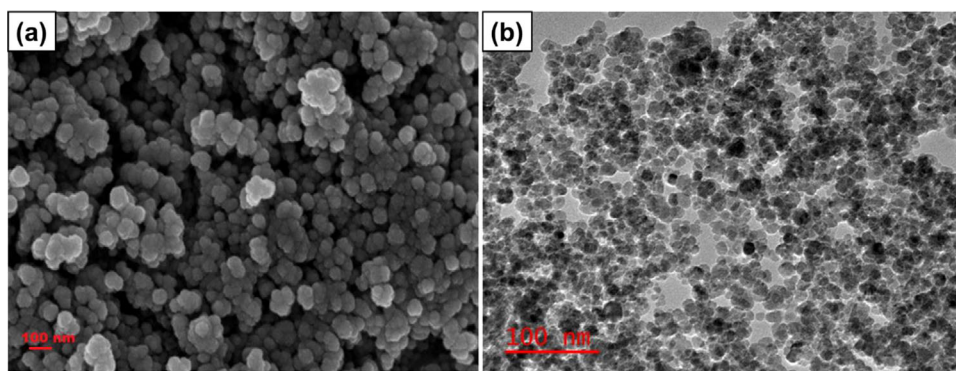


**FIGURE 3** | Field-emission scanning electron microscopy (FE-SEM) (a) and transmission electron microscopy (TEM) (b) micrographs of  $\text{Fe}_3\text{O}_4$  nanoparticles.

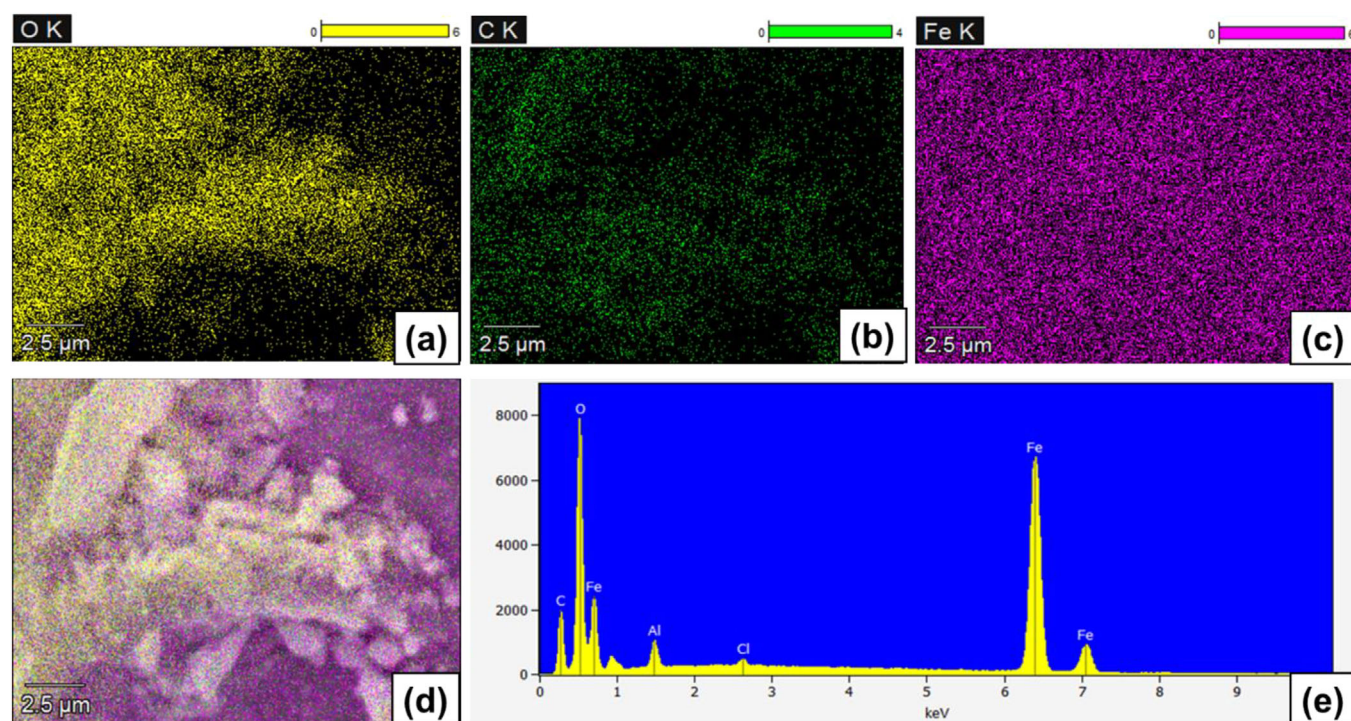


**FIGURE 4** | Energy dispersive X-ray spectroscopy (EDX) Mapping of C (a), Fe (b), O (c), overall mapping image (d), and the EDX spectra (e) of the synthesized  $\text{Fe}_3\text{O}_4$  nanoparticles.

the nanoparticles will better interact with the analytes of interest as there will be more surface interaction. The particles ranged from 2 to 12 nm, with an average particle size of 7 nm. This suggests that the synthesis method could yield low and uniformly sized nanoparticles, which would be ideal for interaction with the analytes. The average particle size attained agreed with the XRD attained average particle size.

### 7.1.3 | EDX Mapping and Spectra

The EDX mapping was done to evaluate the surface distribution of atoms within the synthesized  $\text{Fe}_3\text{O}_4$  nanoparticles. Though carbon Figure 4a was expected to be low on the surface as it was only used for coating, it is noteworthy that the overall surface was populated with Fe atoms (when comparing the individual

Fe atoms in Figure 4b and the overall in Figure 4d. This is followed by oxygen atoms distributed in most parts of the overall  $\text{Fe}_3\text{O}_4$  nanoparticles surface, as shown in Figure 4c, comparable to Figure 4d. The overall surface interaction in Figure 4d suggests that the Fe-O bonds were dominant on the surface of the nanoparticles, which agrees with the FTIR observation. Interestingly, the EDX spectra in Figure 4e show that Fe (65%) and O (19%) were dominant on the surface of the nanoparticles. The remaining distribution was on C (14%) used for coating the surface to avoid charging of the nanoparticles, Al (1%) emanating from the sample stabs, and the negligible distribution from Cl (0.4%) that could be remnants from the salts that were not washed away during the synthesis process. The presence of Fe at various energies suggests their presence in various oxidation states (mostly  $\text{Fe}^{2+}$ ,  $\text{Fe}^{3+}$ , and metallic Fe) that represent the octahedral and tetrahedral states observed in the FTIR.

## 7.2 | Adsorption Studies

### 7.2.1 | Adsorptive Removal of As and Cr From Aqueous Media

To gain insights into the optimal removal of As and Cr in water using  $\text{Fe}_3\text{O}_4$  nanoparticles, various factors, including pH, adsorbent mass, and ultrasonication time, affecting the adsorption of As and Cr onto  $\text{Fe}_3\text{O}_4$  nanoparticles were examined. Notably, the percentage removal of As and Cr can be controlled by varying these parameters. For instance, varying the pH of the solutions had a greater impact on the adsorptive removal of both As and Cr, as shown in Figure S1. The highly protonated form of As at below pH 4 and the highly alkaline form at pH above 9 have been reported to have great mobility and are most stable under neutral conditions [39]. As arsenic is mostly stable around the neutral pH, the highest adsorption recovery is expected. Expectedly, the highest As percentage removal was observed around pH 6.2, yielding a 96% removal in aqueous solutions. On the other hand, Cr removal was favorable at a pH of 7.5, yielding an 86% removal. It is noteworthy that around the pH of 6–8, the cationic Cr dihydroxide forms [40], leading to high removals with  $\text{Fe}_3\text{O}_4$  nanoparticles. Therefore, pH levels of 6.2 and 7.5 were optimal for removing As and Cr, respectively.

The adsorbent mass and the ultrasonication times were simultaneously assessed and were observed to impact the adsorption of As and Cr in aqueous environments. Notably, adsorption was rapid in the first 20 min sonication times for all adsorbent masses (20–120 mg) for As adsorption, as shown in Figure S2. However, the adsorbent mass of 70 mg was found to yield a maximum As adsorption of 92% at the sonication time of 30 min and a pH of 6.2. This implies that the optimum mass was 70 mg, and the ultrasonication time was 30 min for the adsorption of As onto magnetite. On the other hand, the adsorption of Cr was seen to be rapid in the first 25 min sonication times for all adsorbent masses Figure S3. However, at the mass of 50 mg, the maximum adsorption was attained at the sonication time of 20 min, reaching 88% at pH 7.5. Though there was a slight reduction in the Cr adsorption at 25 min, the optimum adsorbent mass and sonication times yielding high adsorption onto magnetite were 50 mg and 20 min, respectively.

### 7.2.2 | Adsorption Isotherms

Following the attainment of the optimum adsorption conditions for As onto magnetite as mass = 70 mg, pH = 6.2, and sonication time = 30 min, as well as Cr onto magnetite as mass = 50 mg, pH = 7.5 and sonication time = 20 min; these conditions were then used to study the adsorption isotherms. Four adsorption isotherms were studied, which included the Langmuir, Freundlich, Sips, and Redlich-Peterson isotherms. The results for fitting these linear isotherm models are shown in Table 1 and Figures S4 and S5.

Table 1 illustrates the summary of parameters for Langmuir, Freundlich, Sips, and Redlich-Peterson attained from isotherm linear models illustrated in Figures S4 and S5 for As and Cr, respectively. These models explain what happens at equilibrium

**TABLE 1** | Adsorption isotherms for arsenic (As) and chromium (Cr) adsorption in aqueous solutions.

Isotherm	Parameters	
	As	Cr
Langmuir		
Slope	0.016	0.019
Intercept	0.049	0.076
$q_{\max}$ (mg/g)	59.9	50.2
KL	1	1
RL	0.065–0.17	0.010–0.17
$R^2$	0.9772	0.9908
Freundlich		
Slope	0.442	0.416
Intercept	1.19	2.39
n	2.26	2.41
Kf	15.74	24.92
$R^2$	0.9541	0.9023
Sips		
Slope	1.18	1.08
Intercept	1.89	1.38
Ks	2.24	1.49
$q_{\max}$ (mg/g)	5.87	12.85
ns	1.88	1.38
$R^2$	0.9615	0.8833
Redlich–Peterson		
Slope	0.970	0.951
Intercept	2.75	2.39
A	2.75	2.39
$\beta$	0.97	0.95
$\alpha_{\text{RP}}$	1.01	0.87
$R^2$	0.9706	0.9506

when the adsorbates (As and Cr) and adsorbent are in contact, as represented in Figures S4a and S5b. The correlation coefficient ( $R^2$ ) and other parameters were used to determine which model best fits the adsorption process. From Table 1, it was indicated that Cr and As best fitted the Langmuir model since the  $R^2$  values (As: 0.9772 and Cr: 0.9908, from Figures S4b and S5b, respectively) were higher than the Freundlich  $R^2$  values (As: 0.9541 and Cr: 0.9023 from Figures S4c and S5c, respectively). This demonstrated that the adsorption mechanism of As and Cr on the surface of the adsorbent happened in a monolayer pattern and was also homogenous. Hence, a Langmuir constant KL of 1 L/g and the maximum adsorption capacities of 59.9 mg/g for As and 50.2 mg/g for Cr were found. Moreover, the separation factor (RL) of 0.065–0.170 for As and 0.010–0.170 for Cr indicated a favorable adsorption process through the Langmuir isotherm. The Sips model was also incorporated to further understand the adsorption processes' nature, as demonstrated in Figures S4d and S5d, respectively. When the Sips model exponent (ns) is

equivalent to 1, the adsorption processes fit Langmuir, and when the exponent (ns) is greater than 1, the data fit the Freundlich model. In this study, the exponent (ns) for As was 1.88, and for Cr was 1.38, which indicated that it fit the Freundlich model and disagreed with the Langmuir isotherm results. This implied that though the homogenous adsorption process was favored, some heterogeneous adsorption could still play a role in the overall adsorption process. The Redlich-Peterson model (Figures S4e and S4e) combines the Langmuir and Freundlich models; in this model, the focus is on the exponent from the plots ( $\beta$ -value); if this value is zero, it reduces to the Freundlich model whilst it reduces to Langmuir if it is 1. From the findings obtained in Table 1,  $\beta$  had a value of 0.97 for As and 0.95 for Cr, which is approximately 1. This indicated that the Langmuir model was favored in explaining the interaction between the adsorbent and the absorbates (As and Cr).

### 7.2.3 | Adsorption Kinetics

To gain insights into the adsorption kinetics of As and Cr in aqueous solutions, batch experiments were conducted using 70 mg (As) and 50 mg (Cr) of  $\text{Fe}_3\text{O}_4$  nanoparticles, pH of 6.2 (As) and 7.5 (Cr) at room temperature (23°C), with the kinetic graph shown in Figures S6a and S7a, for As and Cr, respectively. Notably, the rapid uptake of As by the magnetite adsorbent was evident between 5 and 10 min and a second region of increase between 10 and 30 min, with the resultant equilibrium between 30 and 40 min. The rapid uptake of Cr by the magnetite adsorbent was evident between the first 25 min, with the resultant equilibrium attained in 30 min. The kinetics data were fitted to Pseudo-first order (Figures S6b and S7b) and Pseudo-second order (Figures S6b and S7c) linear kinetic models. Three postulations should be met for the kinetic model to be representative of the data obtained: (1) there should be a good linear relationship such that the trendline should pass through most of the points, (2) the  $q_e$  (experimental) and  $q_e$  (calculated) should be close to each other, (3) the coefficient of determination ( $R^2$ ) should be close to 1 [12, 41]. In both As and Cr models, the pseudo-first-order model trendline did not pass through most of the points, had the experimental  $q_e$  that was not close to the calculated  $q_e$ , and  $R^2$  was not close to 1, suggesting that the adsorption of As and Cr onto magnetite was not an ideal first-order reaction. On the other hand, the pseudo-second-order model trendline passed through most of the points, had the experimental  $q_e$  that was close to the calculated  $q_e$ , and  $R^2$  was close to 1, suggesting that the pseudo-second-order model best described the kinetic equilibrium as it followed the second order reaction. The results suggest that the adsorption process of As followed a chemisorption mechanism involving the electrostatic interaction between the positive surface of the adsorbent and the As oxyanions. The same conclusion could be made for Cr, which showed similar results.

### 7.3 | Seasonal Variation of the Trace Metal Concentrations

Employing the optimum conditions (pH, adsorbent mass, and sonication time) attained for As and Cr, the influence of the physicochemical parameters and the seasonal variation impact

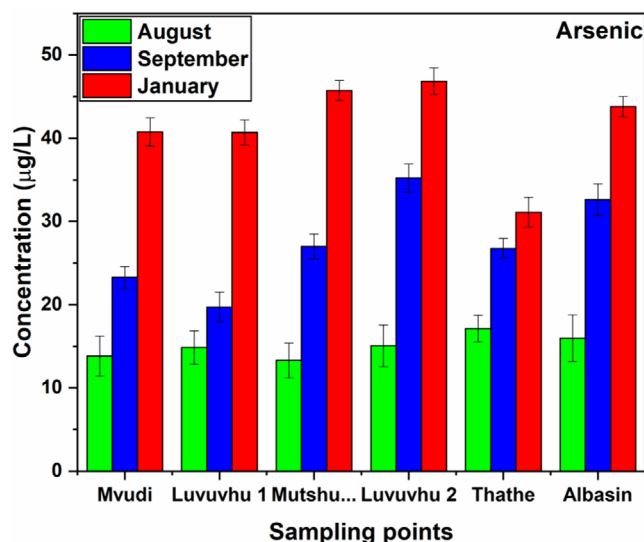


FIGURE 5 | Mean concentrations of arsenic (As) in selected water sources.

on the concentration of As and Cr in various surface water sources in Thulamela and Makhado municipalities were evaluated. The mean concentrations of As ranged from 13.3 to 46.8 µg/L (Table 2) in the river and dam water samples around Thohoyandou. The bar graph in Figure 5 shows the seasonal variation of As at various sampling sites. Interestingly, at all the sampling points, the concentration of As shows an increasing seasonal trend, with the concentrations in January mostly doubling those observed in August. The seasonal comparison of As concentration between the dry season (August), semi-wet season (September), and wet season (January) shows an increasing trend in concentration that may be ascribed to the wash-off of toxins from the surface of the soil to nearby rivers. Worryingly, even though the lowest As concentration of 13.3 µg/L was detected at Mutshundudi River in August, this concentration exceeds the South African National Standard (SANS) and WHO threshold value (10 µg/L) for domestic water use [42]. The highest concentrations of As were recorded near Luvuvhu 2 and Mutshundudi rivers, as well as the Albasin dam, which is in the neighborhood of formal and informal wood preservation plants. Though the reason for these high As concentrations is not clear, knowing the history of using chromate-copper-arsenate (CCA) as an industrial wood preservative in South Africa, the potential of CCA leading to high As concentrations cannot be ruled out [43, 44]. Instead, both sediments and surface water near the wood preservation plants must be systematically investigated to ascertain the potential sources of the high As concentration [45]. Furthermore, the residential areas surrounding these water sources are full of large farms and agricultural lands that use various fertilizers, pesticides, and insecticides for various agricultural activities [46]. Amongst many other activities, cattle dipping is one of the strongest contenders that might lead to the deposition of some metals, particularly As, as it is reported to deal with ticks that are problematic to farmers [47]. Given the reliance of most of the residential areas around the sampling points on farming, particularly cattle farming, cattle dipping using trace metal-containing pesticides might be one of the reasons for the high As concentration levels. Since the average levels of As obtained in this study exceed the guideline values,

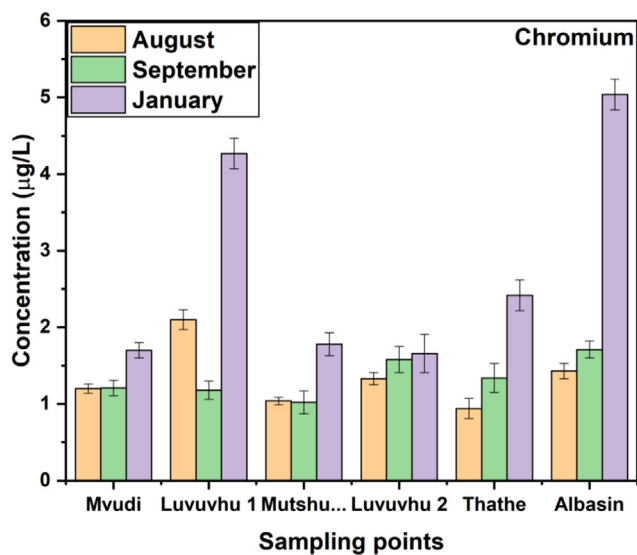


TABLE 2 | The mean concentrations (µg/L) of arsenic (As) and chromium (Cr) in river and dam water in the Thulamela and Makhado municipalities.

Sampling season	Sampling points	As calibration	As concentration (µg/L)	% RSD (As)	Cr Calibration	Cr concentration (µg/L)	% RSD (Cr)
August	Mvudi	$r^2 = 0.9968$	$13.8 \pm 0.03$	3.4	$r^2 = 0.9983$	$1.22 \pm 0.09$	0.063
	Luvuvhu 1	CC (µg/L) = 2.75	$14.9 \pm 0.1$	2.0	CC (µg/L) = 0.130	$2.10 \pm 0.1$	0.14
	Mutshundudi	LOD (µg/L) = 0.09	$13.3 \pm 0.2$	3.1	LOD (µg/L) = 0.07	$1.04 \pm 0.5$	0.052
	Luvuvhu 2	LOQ (µg/L) = 0.27	$15.1 \pm 0.3$	3.5	LOQ (µg/L) = 0.21	$1.33 \pm 0.1$	0.087
	Thathe	Linearity (µg/L) = 0.27–70	$17.1 \pm 0.01$	3.6	Linearity (µg/L) = 0.21–70	$0.94 \pm 0.01$	0.13
September	Albasin		$15.9 \pm 0.1$	2.8		$1.43 \pm 0.1$	0.11
	Mvudi	$r^2 = 0.9998$	$23.3 \pm 0.9$	1.3	$r^2 = 0.9998$	$1.21 \pm 0.3$	0.071
	Luvuvhu 1	CC (µg/L) = 7.15	$19.7 \pm 0.1$	1.8	CC (µg/L) = 0.223	$1.18 \pm 0.07$	0.14
	Mutshundudi	LOD (µg/L) = 0.1	$26.9 \pm 0.1$	1.5	LOD (µg/L) = 0.03	$1.02 \pm 0.2$	0.095
	Luvuvhu 2	LOQ (µg/L) = 0.33	$35.2 \pm 0.4$	1.7	LOQ (µg/L) = 0.16	$1.58 \pm 0.1$	0.24
January	Thathe	Linearity (µg/L) = 0.33–70	$26.7 \pm 0.1$	1.2	Linearity = 0.16–70	$1.34 \pm 0.04$	0.22
	Albasin		$32.6 \pm 0.3$	1.9		$1.71 \pm 0.1$	0.13
	Mvudi	$r^2 = 0.9983$	$40.8 \pm 0.06$	2.4	$r^2 = 0.9990$	$1.71 \pm 0.05$	0.16
	Luvuvhu 1	CC (µg/L) = 3.30	$40.7 \pm 0.1$	3.5	CC (µg/L) = 0.112	$4.27 \pm 0.1$	0.22
	Mutshundudi	LOD (µg/L) = 0.1	$45.73 \pm 0.9$	4.8	LOD (µg/L) = 0.05	$1.78 \pm 0.9$	0.14
	Luvuvhu 2	LOQ (µg/L) = 0.34	$46.85 \pm 1.4$	2.4	LOQ (µg/L) = 0.18	$1.66 \pm 0.1$	0.11
	Thathe	Linearity (µg/L) = 0.33–70	$31.10 \pm 0.09$	3.8	Linearity (µg/L) = 0.18–70	$2.42 \pm 1.1$	0.23
	Albasin		$43.81 \pm 0.1$	3.2		$5.04 \pm 0.09$	0.21

Abbreviations: CC = characteristic concentration; LOD = limit of detection; LOQ = limit of quantification, RSD = relative standard deviation.





**FIGURE 6** | Concentrations of chromium (Cr) in selected water sources.

consuming As-rich water could harm human health. As noted, most people residing in rural areas that lack municipal water depend on untreated surface water from the Mutshundudi and Luvuvhu rivers for domestic use [48], shown in Table 2 to have very high levels of As. This may lead to various adverse health effects on the communities and animals utilizing this water for domestic purposes.

The mean concentration of Chromium in Table 2 ranged from 1.02 to 5.04 µg/L, which was below the SANS and WHO threshold values of 50 µg/L [49], respectively, for domestic water use. The seasonal variation was represented using the bar graph in Figure 6. It is noteworthy that the concentrations in August were equivalent to those observed in September, except for Thathe dam, which has shown a spike in concentration, possibly as a result of wastewater discharges from the tea plantation in Thathe. Interestingly, in January, when there was rainfall and stormwater runoff, Cr concentrations increased at an alarming rate, especially in Luvuvhu 1 river point and Albasin Dam, which are located in areas where wood preservation industries are located. Though the concentrations of Cr were not as high as As in the same regions, it might be possible that Cr was transferred from water to sediments. Nonetheless, the anticipated use of CCA for wood preservation cannot be ruled out. Therefore, this requires the analysis of both surface water and sediments near the wood treatment plants.

#### 7.4 | Seasonal Variation on the Rivers and Dams Physicochemical Properties

The pH of the water sample plays an important role in the metal bioavailability, leaching, and toxicity to surrounding areas, especially when the seasonal variation is considered [50]. It has been reported that for most metals, an increase in the pH of the solution causes a decrease in their concentration [51]. As seen in Figure 7 and Table 3, an increase in pH promotes a decrease in As and Cr concentrations. The slight change in

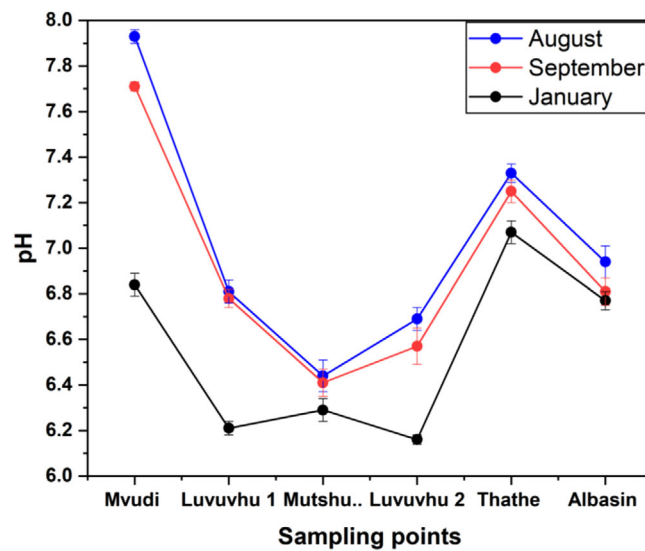


**FIGURE 7** | pH variation at different sampling points and various sampling seasons.

pH on the samples collected in the winter (August) to early summer (September) suggests a slight increase in As and Cr concentrations. Trace metals are mostly soluble and leach out in acidic pH [51]. The metals are also mostly bioavailable in water during the rainy season as they are easily washed off and less absorbed by plants and sediments [52]. Expectedly, during the late summer season (January), there is a significant increase in As and Cr concentrations shown by the reduction in pH from alkaline to acidic pH, which can be ascribed to the trace metals washed off from the surface and deposited into the nearby water sources. The high dilution of trace metals is expected when the water volume and flow increase, which influences the concentration of metals during the wet season [53]. This implies that high concentrations will be detected in the dry season and low concentrations in the wet season [54, 55]. Nevertheless, trace metal levels in surface water are fundamentally induced by storm water run-off emanating from the surrounding topsoil wash-off to nearby river and dam catchments, which leads to an increase in trace metal concentration during the wet season [56]. Unsurprisingly, due to a possible stormwater runoff during the rainy season, the pH decreased in all rivers, as shown in Figure 7. The pH at the two dams (Thathe and Albasin) also shows a noteworthy decrease in pH, even though the high dilution factor was expected to play a role in ensuring there was an insignificant decrease in pH, if not an increase [53]. The water quality regulations postulate that the drinking water should have a pH level of 6.5–9.5, as shown in Table 3. According to the results obtained in Figure 7, all the rivers satisfy this, except the Mutshundudi River in August and September. However, when it was raining in January, both Mutshundudi and Luvuvhu rivers were below the recommended pH values, as shown in Table 3. Interestingly, both rivers pass through wood treatment plants, which might have impacted the pH range observed.

The TDS represent the total amount of dissolved substances in water, such as metal ions, high-solubility minerals, soluble salts, and exchangeable ions [60–62]. Expectedly, the TDS amount in freshwater is usually at less than 500 ppm, as the lower the

**TABLE 3** | Acceptable pH levels according to the World Health Organization (WHO), United States Environmental Protection Agency (USEPA), and South African National Standard (SANS) [57–59].

pH in water (at 25°C)	Suitability for drinking water	WHO guideline	USEPA guideline	SANS 241 guideline
7–7.9	Excellent	6.5–8.5	6.5–8.5	5–9.7
6–6.9	Most acidic, good for drinking water			
8–9	Most alkaline, good for drinking water			
>9 and 6<	Not recommended for drinking			

**TABLE 4** | Total dissolved solids (TDS) acceptable levels in drinking water according to the World Health Organization (WHO), the United States Environmental Protection Agency (USEPA), and the South African National Standard (SANS) [57–59].

TDS in water (mg/L)	Suitability for drinking water	WHO guideline	USEPA guideline	SANS 241 guideline
50–149	Excellent for drinking	TDS below 300 mg/L is considered safe for drinking.	TDS below 500 mg/L is considered safe for drinking.	TDS ≤ 1200 mg/L is considered safe for drinking.
150–249	Good for drinking			
250–299	Fair for drinking			
300–500	Poor, not good for drinking			
Above 1200	Unacceptable			

TDS, the better the water for drinking, as reported in Table 4. As they are not fit for drinking, seawater often contains about 500–30 000 ppm [49]. Though some dissolved substances in water emancipate from natural sources, anthropogenic sources such as sewage, urban run-offs, industrial wastewater, agricultural chemical fertilizers, and chemicals from wastewater treatment processes are often responsible for the increase in TDS [63], which renders the water not good for drinking. The seasonal variation of the TDS measurements is critical in evaluating the water quality, especially the water hardness, as high TDS describes the increased water hardness [64]. Moreover, TDS is one of the critical factors in measuring water quality and impacts chemical transformation, mass transport, and ionization of metals in water [65]. The TDS results in all the catchments studied in Figure 8 were within the water quality standards provided by the WHO, the United States Environmental Protection Agency (USEPA), and SANS (Table 4). As in the case of the pH evaluations, the TDS increasing trend was observed from August to January, with January showing the highest TDS values. The seasonal variation shows that during the rainy season, the water is harder than in the winter, as stormwater runoff deposits more substances that were previously on the surface of the topsoil into nearby rivers and dams, as shown by the TDS trend in Figure 8.

Electrical conductivity represents the measure of the ability of water to conduct an electric current due to the presence of conducting ions such as nitrates, potassium, chloride, magnesium, carbonate, sulfate, bicarbonate, sodium, and calcium, amongst others [66]. Though most ions are available in the environment naturally, anthropogenic sources increase their concentrations and, therefore, their conductivity [7]. It has been reported that water with a conductivity of above 800  $\mu\text{S}/\text{cm}$  is considered hard, which is reflected in Table 5. Notably, according to the SANS

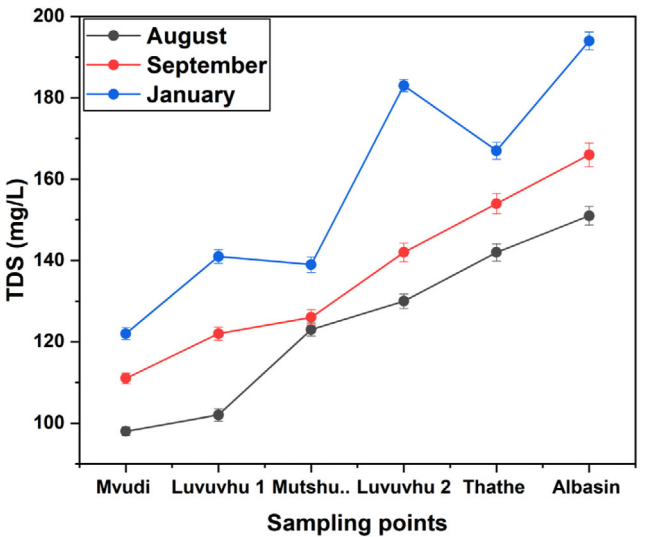


**FIGURE 8** | Total dissolved solids assessments at different sampling points and various sampling seasons.

guideline in Table 5, the EC observed in all surface water evaluated is above the threshold value of 170  $\mu\text{S}/\text{cm}$ . Nonetheless, the water from all the rivers and dams (Figure 9) is within the WHO threshold of 400  $\mu\text{S}/\text{cm}$  and can be deemed safe for drinking per the WHO guidelines. However, the continued increase in EC indicated the increase in both As and Cr concentrations, which raises the alarm about how much more As and Cr is available in sediments, plants, and soil. The USEPA guidelines cannot be used to validate and support the results obtained as it is above 800  $\mu\text{S}/\text{cm}$ , which is now considered hard water.

**TABLE 5** | Electrical conductivity (EC) guidelines in drinking water according to the World Health Organization (WHO), the United States Environmental Protection Agency (USEPA), and the South African National Standard (SANS) [59, 67, 68].

EC in water ( $\mu\text{S}/\text{cm}$ )	Suitability for drinking water	WHO guideline	USEPA guideline	SANS 241 guideline
0–800	Good drinking water for humans	Should not	Less than	$\text{EC} \leq 170 \mu\text{S}/\text{cm}$
800–2500	Can be consumed by humans although recommendations favor water in the lower half of the range	exceed $400 \mu\text{S}/\text{cm}$ to be	$1000 \mu\text{S}/\text{cm}$ for	is considered
2500–10,000	Not recommended for human consumption	considered safe	drinking water	safe for drinking.
Above 10,000	Unacceptable, not suitable for human consumption	for drinking		

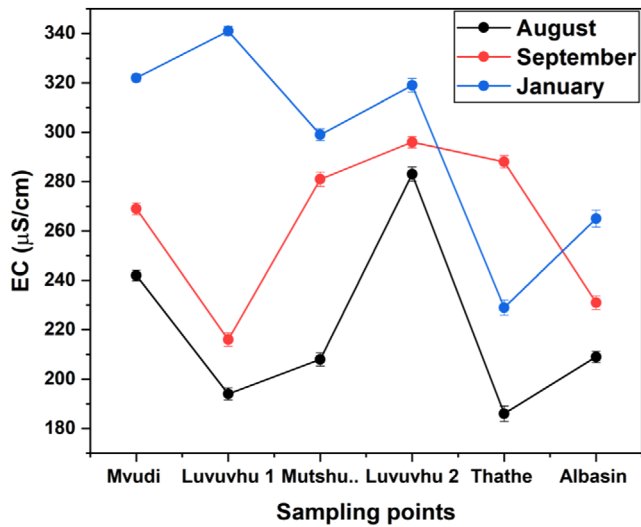


**FIGURE 9** | Electrical conductivity assessments at different sampling points and various sampling seasons.

### 7.5 | Quality and Statistical Analysis

Calibration standards were prepared using analytical grade chemicals and ultrapure water to ensure that QA and control were observed. Furthermore, after analyzing every 20 samples, the  $100 \mu\text{g}/\text{L}$  freshly prepared Pd standard was analyzed in triplicates as a chemical matrix modifier. This eliminated chemical matrix impacts anticipated to interfere with the analysis program. The RSD of each group of replicate samples was determined to be below 5% for all the metals, alongside maintaining the linear calibration graphs with coefficients above 0.99 for both As and Cr, confirming an excellent response from the analytes. Furthermore, the LOD, LOQ, and linearity of both As and Cr were summarised in Table 2, with the results confirming the analytes' excellent response towards the GFAAS instrument. The characteristic concentration results in Table 2 demonstrate that the instrument was more sensitive in the September analysis but still displayed an acceptable sensitivity in August and January. The samples of interest were analyzed in triplicates, and the standard deviations were calculated in every sampling point, as shown in Table 2 and Figures 5 and 6.

Seasonally, higher concentrations of As and Cr were observed in the wet season compared to the dry season, as observed in Figures 5 and 6, respectively. Statistical analysis ( $p < 0.05$ ) showed a significant variation in pH in the Mvudi, Luvuvhu 1, and Luvuvhu 2 rivers but a small variation in the Mutshundudi River, Thathe, and Albasin dams. The latter might have resulted from high dilution factors as these sources were at total capacity in the wet season, resulting in a negligible change in the pH. The temperature changes of only  $5$  to  $10^\circ\text{C}$  in river or dam water may cause detectable changes in TDS values [69]. Similarly, the mean difference in TDS of the water varied significantly ( $p < 0.05$ ) in the wet and dry season. The only correlation observed was in September at the Mutshundudi River, with a negligible change in TDS. The rest of the TDS readings showed a significant variation in TDS between the August, September, and January samples. Water evaporates during the dry season, and the concentration of ions increases hence, EC increases [69]. To this end, the mean difference in the EC of the water varied significantly ( $p < 0.05$ ) in the wet and dry seasons. However, EC showed increasing trends from dry to wet season, resulting from the possible high flow of stormwater that might have deposited more ions from the soil surface into the water sources. Surprisingly, a lower EC was observed in the Thathe dam in January compared to September. This may have resulted from the dilution of ions as the dam receives large volumes of water from various rivers during the wet season.

### 7.6 | Possible Sources of Trace Metals within the Study Area

Though Cr concentrations were below the permissible limits, the concentrations of As were alarming as they were above the permissible limits in all rivers and dams studied. The high concentrations of As might be related to the historical use of CCA for wood preservation in the area; however, with the low concentrations of Cr, sediment analysis in water and soil analysis near wood preservation industries would need to be assessed. This could be coupled with the speciation of both As and Cr in water samples to give a more detailed analysis of the more available species in water samples [70, 71]. Nonetheless, the high concentration of As detected in the Luvuvhu ( $46.9 \mu\text{g}/\text{L}$ ) and Mutshundudi ( $45.7 \mu\text{g}/\text{L}$ ) rivers that pass across wood-preserving industries was alarming. Furthermore, cattle dipping facilities

**TABLE 6** | Chronic daily intakes (CDIs, mg/kg day) of trace metals obtained from the rivers and dams.

Elements	Season	Sampling points						RfD
		Mvudi	Luvuvhu1	Mutshundudi	Luvuvhu2	Thathe	Albasin	
As	Wet	18.8	20.4	19.7	16.7	20.4	17.7	0.301
	Dry	40.8	35.9	25.9	16.9	21.7	23.9	
Cr	Wet	1.33	1.04	0.942	1.22	1.15	1.09	3.00
	Dry	1.22	1.02	1.34	1.98	2.67	2.42	

**TABLE 7** | Incremental lifetime cancer risk of As and Cr (mg/kg per day).

Elements	Mvudi	Luvuvhu 1	Mutshundudi	Luvuvhu 2	Thate	Albasini
As	$3.01 \times 10^{-2}$	$3.02 \times 10^{-2}$	$3.34 \times 10^{-2}$	$2.91 \times 10^{-2}$	$3.40 \times 10^{-2}$	$5.01 \times 10^{-2}$
Cr	$1.79 \times 10^{-5}$	$1.10 \times 10^{-5}$	$1.11 \times 10^{-5}$	$1.56 \times 10^{-5}$	$1.71 \times 10^{-5}$	$1.62 \times 10^{-5}$

have also been observed in the Vhembe municipality, as cattle farming is one of the key economic drivers within the area, which might be a potential source of As. Besides cattle farming, other agricultural activities, such as the irrigation of crops, are dominant in the area, which might lead to the possibility of the use of As-containing pesticides and insecticides. Interestingly, chicken farming was observed in the area, with chicken feed as one of the possibilities for introducing As in the studied area. Analysing soil samples near the chicken farming yard would be necessary to ensure the high As concentrations detected are not associated with chicken farming in the area. The sewage system is also one of the possibilities for introducing Cr in water sources as most of the rural areas studied here lack proper sanitary services and often use pit latrines in their homes.

## 7.7 | Health Risk Assessment

### 7.7.1 | Chronic Daily Intake of Trace Metals

Based on the results, the chronic daily intakes (CDIs) for As in river and dam water collected during the wet season were 16.7 to 20.5, as shown in Table 6. The CDIs for As in the river and dam water collected during the dry season were 16.9–40.8. The CDIs for Cr were in the range of 0.942–1.33 for the wet season, and for the dry season, it was in the range of 1.02–2.67. Table 6 shows that the CDIs of trace metals varied during the dry and wet seasons. Moreover, As CDI values were higher than the corresponding oral reference dose (RfD). An RfD value is the estimated value per day of exposure to a certain metal in the human body that has no hazardous effect during a lifetime [33]. It was concluded that As posed severe health threats to the communities within the study area due to all their CDI values exceeding the RfD value. On the other hand, Cr posed no health threats at the current levels as the CDI values were lower than the RfD values. Furthermore, the literature shows trace amounts of As and Cr threaten human health [10]. For instance, excessive exposure to As has been reported to cause skin lesions, cancer, neurological issues, and abdominal pains, amongst others [13]. Subsequently, Cr is also known to be unsafe to human and marine life, but

this depends on the concentration and species, which is still low within the study area but rising seasonally [33].

### 7.7.2 | Carcinogenic Risk

The carcinogenic risk caused by As and Cr in river water samples was obtained by determining the incremental lifetime cancer risk (ILCR), as shown in Table 7. The ILCR readings of the carcinogens of interest were obtained to be higher than the acceptable limit of  $1.00 \times 10^{-4}$  mg/kg per day for As, but lower than  $1.00 \times 10^{-6}$  mg/kg per day for Cr. It is clearly illustrated that As has a crucial role in the carcinogenic risk of the study areas as it reported the highest ILCR levels compared to Cr. The findings suggested that As can cause serious negative impacts on living organisms in the study areas, as the daily consumption of untreated river and dam water may cause various diseases.

## 8 | Conclusion

The current study examined seasonal variations in the concentrations of As and Cr, along with their impacts on water quality. To facilitate the adsorption of As and Cr from water and enhance their detection, highly dispersed  $\text{Fe}_3\text{O}_4$  nanoparticles were utilized. The research evaluated four rivers and two dams, noting that seasonal changes significantly influenced both the metal concentrations and water quality. In the study area, As levels ranged from 13.3 to 46.9  $\mu\text{g/L}$ , while Cr concentrations varied from 1.02 to 5.04  $\mu\text{g/L}$ . Although Cr levels were low, As concentrations exceeded the acceptable limits set by the WHO and SANS. As the concentrations of these metals increased, there were notable changes in water quality. Parameters such as pH, EC, and TDS were found to influence the concentrations of As and Cr. Seasonal variations indicated lower pH levels, higher EC and TDS at increased metal concentrations, and vice versa. Primary anthropogenic activities, including agriculture and industrialization, are suspected contributors to the elevated As levels observed. The health assessment indicated that the CDI for As in water collected from the rivers and dams during the wet season ranged from 16.7 to 20.5, while during the dry season, it



ranged from 16.9 to 40.8. The CDIs for Cr were measured at 0.942 to 1.33 in the wet season and 1.02 to 2.67 in the dry season. The results revealed that As CDI values exceeded the corresponding RfD, suggesting serious health risks for communities in the area, as all CDI values surpassed the RfD. Additionally, the ILCR for As was found to be higher than  $10^{-6}$  mg/kg per day, which is deemed unacceptable, while Cr levels remained below  $10^{-4}$  mg/kg per day, with these results consistent with the CDI results. Since surface water is commonly used for drinking in the study area, it is crucial to further evaluate the sediments and soil to mitigate potential health risks that may affect the rural communities reliant on the assessed rivers and dams.

## Author Contributions

**Tshimangadzo S. Munonde:** investigation, conceptualization, supervision, methodology, formal analysis, resources, writing—original draft. **Shirley K. Selahle:** writing and review, investigation, resources.

## Acknowledgements

The authors would like to thank the University of Venda for funding and access to laboratory equipment, and the late Mr Paul E.L Mojapelo of the University of Venda (South Africa) for assistance in the analysis of the water samples. The University of South Africa is thanked for the provision of manpower and access to laboratory equipment. Mr Gavin Mukweho is also acknowledged for his assistance with the collection of water samples.

## Conflicts of Interest

The authors declare no conflicts of interest.

## Data Availability Statement

The authors declare that the data supporting the findings of this study are available within the paper and its Supporting Information files.

## References

1. T. Kimura and M. Ikoma, "Predicted Diversity in Water Content of Terrestrial Exoplanets Orbiting M Dwarfs," *Nature Astronomy* 6 (2022): 1296–1307.
2. K. Dharmasastha, Z. Zhong, J. Niu, and H. Liang, "A Comprehensive Review of Cover-Shield-Assisted Radiant Cooling System," *Energy and Buildings* 291 (2023): 113121.
3. S. Wang, X. Wang, and S. Chen, "Global Value Chains and Carbon Emission Reduction in Developing Countries: Does Industrial Upgrading Matter?" *Environmental Impact Assessment Review* 97 (2022): 106895.
4. J. O. Alao, A. Fahad, H. G. Abdo, et al., "Effects of Dumpsite Leachate Plumes on Surface and Groundwater and the Possible Public Health Risks," *Science of the Total Environment* 897 (2023): 165469.
5. A. Tariq and A. Mushtaq, "Untreated Wastewater Reasons and Causes: A Review of Most Affected Areas and Cities," *International Journal of Chemical and Biochemical Sciences* 23 (2023): 121–143.
6. I. Chakravarty, A. Bhattacharya, and S. K. Das, "Water, Sanitation and Hygiene: The Unfinished Agenda in the World Health Organization South-East Asia Region," *WHO South-East Asia Journal of Public Health* 6 (2017): 22–26.
7. N. Akhtar, M. I. Syakir Ishak, S. A. Bhawani, and K. Umar, "Various Natural and Anthropogenic Factors Responsible for Water Quality Degradation: A Review," *Water* 13 (2021): 2660.
8. M. Cetin, A. M. O. Aljama, O. B. M. Alrabiti, F. Adiguzel, H. Sevik, and I. Zeren Cetin, "Determination and Mapping of Regional Change of Pb

and Cr Pollution in Ankara City Center," *Water, Air, & Soil Pollution* 233 (2022): 163.

9. R. N. Khalef, A. I. Hassan, and H. M. Saleh. Heavy metal's environmental impact (2022).
10. D.-P. Häder, A. T. Banaszak, V. E. Villafañe, M. A. Narvarte, R. A. González, and E. W. Helbling, "Anthropogenic Pollution of Aquatic Ecosystems: Emerging Problems With Global Implications," *Science of the Total Environment* 713 (2020): 136586.
11. P. Sharma, D. Dutta, A. Udayan, A. K. Nadda, S. S. Lam, and S. Kumar, "Role of Microbes in Bioaccumulation of Heavy Metals in Municipal Solid Waste: Impacts on Plant and Human Being," *Environmental Pollution* 305 (2022): 119248.
12. A. S. Gugushe, A. Mpupa, T. S. Munonde, L. Nyaba, and P. N. Nomngongo, "Adsorptive Removal of Cd, Cu, Ni and Mn From Environmental Samples Using Fe<sub>3</sub>O<sub>4</sub>-ZrO<sub>2</sub>@ APS Nanocomposite: Kinetic and Equilibrium Isotherm Studies," *Molecules* 26 (2021): 3209.
13. S. Mitra, A. J. Chakraborty, A. M. Tareq, et al., "Impact of Heavy Metals on the Environment and Human Health: Novel Therapeutic Insights to Counter the Toxicity," *Journal of King Saud University-Computer and Information Sciences* 34 (2022): 101865.
14. M. Balali-Mood, K. Naseri, Z. Tahergorabi, M. R. Khazdair, and M. Sadeghi, "Toxic Mechanisms of Five Heavy Metals: Mercury, Lead, Chromium, Cadmium, and Arsenic," *Frontiers in Pharmacology* 12 (2021): 643972. 227.
15. H. Ali, E. Khan, and I. Ilahi, "Environmental Chemistry and Ecotoxicology of Hazardous Heavy Metals: Environmental Persistence, Toxicity, and Bioaccumulation," *Journal of Chemistry* 2019 (2019): 6730305.
16. M. K. Abd Elnabi, N. E. Elkaliny, M. M. Elyazied, et al., "Toxicity of Heavy Metals and Recent Advances in Their Removal: A Review," *Toxics* 11 (2023): 580.
17. P. Vasistha and R. Ganguly, "Water Quality Assessment of Natural Lakes and its Importance: An Overview," *Materials Today: Proceedings* 32 (2020): 544–552.
18. A. Mishra, J. K. Behera, P. Mishra, M. Bhattacharya, B. Behera, and N. B. Kar, "Risk Assessment of Heavy Metal Contaminations in Soil and Water Ecosystem," in *Soil Health and Environmental Sustainability: Application of Geospatial Technology*, eds. P. K. Shit, P. P. Adhikary, G. S. Bhunia, and D. Sengupta (Switzerland: Springer, 2022), 389–404.
19. P. Maponya, "Opportunities and Constraints Faced by Smallholder Farmers in the Vhembe District, Limpopo Province in South Africa," *Circular Economy and Sustainability* 1 (2021): 1387–1400.
20. E. Ingwani, M. Thynell, L. R. Gurure, et al., "The Impacts of Peri-Urban Expansion on Municipal and Ecosystem Services: Experiences From Makhado Biaba Town, South Africa," in *Proceedings of the Urban Forum* (Switzerland: Springer, 2023), 297–327.
21. P. O. Njoku, O. S. Durowoju, S. E. Uhumamure, and R. Makungo, "Investigating the Attitude of Domestic Water Use in Urban and Rural Households in South Africa," *Water* 14 (2022): 210.
22. M. Rambauli, M. A. Antwi, P. P. Tshikhudo, and F. N. Mudau, "The Determinants of Smallholder Farmers on the Functionality of Plant Health Clinics in the Vhembe District, South Africa," *Agriculture* 13 (2023): 428.
23. M. Nyadzani, P. E. Matshidze, S. L. Kugara, and T. D. Mdhluli, "An Exploration of African Indigenous Knowledge Systems for Nature Conservation in Thohoyandou," *African Journal of Development Studies (formerly AFFRIKA Journal of Politics, Economics and Society)* 13 (2023): 27–54.
24. F. K. S. Mathivha. Evaluating the role of informal waste sector in municipal solid waste management in Vhembe District Municipality, Limpopo Province, South Africa. (2023).
25. J. N. Edokpayi, M. Nkhumeleni, A. M. Enitan-Folami, and F. C. Olaniyi, "Water Quality Assessment and Potential Ecological Risk of Trace Metals in Sediments of some Selected Rivers in Vhembe District,

- South Africa," *Physics and Chemistry of the Earth, Parts A/B/C* 126 (2022): 103111.
26. A. Murei, I. Kamika, A. Samie, and M. N. B. Momba, "Assessment of the Water Sources for Potential Channels of Faecal Contamination Within Vhembe District Municipality Using Sanitary Inspections and Hydrogen Sulphide Test," *Scientific Reports* 13 (2023): 6250.
27. T. T. Phungela, T. Maphanga, B. S. Chidi, B. S. Madonsela, and K. Shale, "The Impact of Wastewater Treatment Effluent on Crocodile River Quality in Ehlanzeni District, Mpumalanga Province, South Africa," *South African Journal of Science* 118 (2022): 1–8.
28. S. Coxon and C. Eaton. Review of contaminants of potential human health concern in wastewater and stormwater. (2023).
29. E. L. Ungureanu and G. Mustatea. Toxicity of heavy metals. (2022).
30. K. Szálkai, "Water-borne diseases," in *The Palgrave Encyclopedia of Global Security Studies*, eds. S. N. Romaniuk and P. Marton (Switzerland: Springer, 2023), 1540–1546.
31. T. S. Munonde, N. W. Maxakato, and P. N. Nomngongo, "Preparation of Magnetic  $\text{Fe}_3\text{O}_4$  Nanocomposites Modified With  $\text{MnO}_2$ ,  $\text{Al}_2\text{O}_3$ , Au and Their Application for Preconcentration of Arsenic in River Water Samples," *Journal of Environmental Chemical Engineering* 6 (2018): 1673–1681.
32. T. S. Munonde, N. W. Maxakato, and P. N. Nomngongo, "Preconcentration and Speciation of Chromium Species Using ICP-OES After Ultrasound-Assisted Magnetic Solid Phase Extraction With an Amino-Modified Magnetic Nanocomposite Prepared From  $\text{Fe}_3\text{O}_4$ ,  $\text{MnO}_2$  and  $\text{Al}_2\text{O}_3$ ," *Microchimica Acta* 184 (2017): 1223–1232.
33. W. A. Khan, M. B. Arain, and M. Soylak, "Nanomaterials-Based Solid Phase Extraction and Solid Phase Microextraction for Heavy Metals Food Toxicity," *Food and Chemical Toxicology* 145 (2020): 111704.
34. J. You, L. Wang, Y. Zhao, and W. Bao, "A Review of Amino-Functionalized Magnetic Nanoparticles for Water Treatment: Features and Prospects," *Journal of Cleaner Production* 281 (2021): 124668.
35. V. Kumar, N. K. Kaushik, S. K. Tiwari, D. Singh, and B. Singh, "Green Synthesis of Iron Nanoparticles: Sources and Multifarious Biotechnological Applications," *International Journal of Biological Macromolecules* 253 (2023): 127017.
36. S. Shukla, R. Khan, and A. Davey, "Synthesis and Characterization of Magnetic Nanoparticles, and Their Applications in Wastewater Treatment: A Review," *Environmental Technology & Innovation* 24 (2021): 101924.
37. T. Rasheed, "Magnetic Nanomaterials: Greener and Sustainable Alternatives for the Adsorption of Hazardous Environmental Contaminants," *Journal of Cleaner Production* 362 (2022): 132338.
38. B. E. Keshta, A. H. Gemeay, D. K. Sinha, et al., "State of the Art on the Magnetic Iron Oxide Nanoparticles: Synthesis, Functionalization, and Applications in Wastewater Treatment," *Results in Chemistry* 7 (2024): 101388.
39. L. Weerasundara, Y.-S. Ok, and J. Bundschuh, "Selective Removal of Arsenic in Water: A Critical Review," *Environmental Pollution* 268 (2021): 115668.
40. S. A. S. Mohammed, "Potential of Surface Complexation and Redox Modeling for Chromium (VI) Adsorption on Local Materials as Liners for Waste Containment Facilities," *Turkish Journal of Engineering and Environmental Sciences* 37 (2013): 100–108.
41. T. S. Munonde, A. Ngombolo, S. Hobongwana, A. Mpupa, and P. N. Nomngongo, "Removal of Methylene Blue Using  $\text{MnO}_2$ @ rGO Nanocomposite From Textile Wastewater: Isotherms, Kinetics and Thermodynamics Studies," *Heliyon* 9, no. 4 (2023): e15502.
42. W. Z. Mandindi, L. Nyaba, N. Mketo, and P. N. Nomngongo, "Seasonal Variation of Drinking Water Quality and Human Health Risk Assessment: A Case Study in Rural Village of the Eastern Cape, South Africa," *Water* 14 (2022): 2013.
43. R. V. Niyobuhungiro. "An Investigation of CCA-Treated Wood in Informal Caterers' Fuel Stocks and Related Airborne Arsenic in the Cape Town Region" (master's thesis, University of Cape Town, 2012).
44. E. Oppong, W. A. Nnuro, I. Ofori, and A. Amaniampong, "Metal Leaching From Chromated Copper Arsenate (CCA)-Treated Wood: Implications on the Environment," *International Journal of Environmental Research* 1 (2021): 14–52.
45. C. C. Osuna-Martínez, M. A. Armienta, M. E. Bergés-Tiznado, and F. Pérez-Osuna, "Arsenic in Waters, Soils, Sediments, and Biota From Mexico: An Environmental Review," *Science of the Total Environment* 752 (2021): 142062.
46. N. M. Nengovhela. "The Use of Cover Crops to Increase Yield and Reduce Pest Pressure in a Commercial Avocado Orchard at Levubu, Limpopo Province" (PhD diss., University of Venda, 2020).
47. A. C. Horn and M. R. Ramudzuli, "Arsenic Contamination of Soil in Relation to Water in Northeastern South Africa," in *Arsenic Water Resources Contamination: Challenges and Solutions*, eds. A. Fares and S. Singh (Cham: Springer, 2020), 157–175.
48. N. Potgieter, S. Karambwe, L. S. Mudau, T. Barnard, and A. Traore, "Human Enteric Pathogens in Eight Rivers Used as Rural Household Drinking Water Sources in the Northern Region of South Africa," *International Journal of Environmental Research and Public Health* 17 (2020): 2079.
49. I. Moffat, N. Martinova, C. Seidel, and C. M. Thompson, "Hexavalent Chromium in Drinking Water," *Journal-American Water Works Association* 110 (2018): E22–E35.
50. A. Gogoi, K. Taki, and M. Kumar, "Seasonal Dynamics of Metal Phase Distributions in the Perennial Tropical (Brahmaputra) River: Environmental Fate and Transport Perspective," *Environmental Research* 183 (2020): 109265.
51. A. Król, K. Mizerna, and M. Bożym, "An Assessment of pH-Dependent Release and Mobility of Heavy Metals From Metallurgical Slag," *Journal of Hazardous Materials* 384 (2020): 121502.
52. L. S. Miranda, G. A. Ayoko, P. Egodawatta, W.-P. Hu, O. Ghidan, and A. Goonetilleke, "Physico-Chemical Properties of Sediments Governing the Bioavailability of Heavy Metals in Urban Waterways," *Science of the Total Environment* 763 (2021): 142984.
53. J. N. Edokpayi, J. O. Odiyo, E. O. Popoola, and T. A. M. Msagati, "Evaluation of Temporary Seasonal Variation of Heavy Metals and Their Potential Ecological Risk in Nzhelele River, South Africa," *Open Chemistry* 15 (2017): 272–282.
54. M. Ahmed, M. Matsumoto, A. Ozaki, N. V. Thinh, and K. Kurosawa, "Heavy Metal Contamination of Irrigation Water, Soil, and Vegetables and the Difference Between Dry and Wet Seasons Near a Multi-Industry Zone in Bangladesh," *Water* 11 (2019): 583.
55. K. N. Abdul Maulud, A. Fitri, W. H. M. Wan Mohtar, W. S. Wan Mohd Jaafar, N. Z. Zuhairi, and M. K. A. Kamarudin, "A Study of Spatial and Water Quality Index During Dry and Rainy Seasons at Kelantan River Basin, Peninsular Malaysia," *Arabian Journal of Geosciences* 14 (2021): 1–19.
56. J. N. Edokpayi, J. O. Odiyo, O. E. Popoola, and T. A. M. Msagati, "Assessment of Trace Metals Contamination of Surface Water and Sediment: A Case Study of Mvudi River, South Africa," *Sustainability* 8 (2016): 135.
57. H. M. A.-S. Yehia and S. M. Said, "Drinking Water Treatment: pH Adjustment Using Natural Physical Field," *Journal of Biosciences and Medicines* 9 (2021): 55–66.
58. R. Islam, S. M. Faysal, R. Amin, et al., "Assessment of pH and Total Dissolved Substances (TDS) in the Commercially Available Bottled Drinking Water," *IOSR Journal of Nursing and Health Science* 6 (2017): 35–40.

59. P. Verlicchi and V. Grillini, "Surface and Groundwater Quality in South African Area—Analysis of the Most Critical Pollutants for Drinking Purposes," in *Proceedings of the Proceedings* (MDPI, 2019), 3.
60. A. A. A. Maliki, A. Chabuk, M. A. Sultan, B. M. Hashim, H. M. Hussain, and N. Al-Ansari, "Estimation of Total Dissolved Solids in Water Bodies by Spectral Indices Case Study: Shatt al-Arab River," *Water, Air, & Soil Pollution* 231 (2020): 1–11.
61. G. E. Adjovu, H. Stephen, D. James, and S. Ahmad, "Measurement of Total Dissolved Solids and Total Suspended Solids in Water Systems: A Review of the Issues, Conventional, and Remote Sensing Techniques," *Remote Sensing* 15 (2023): 3534.
62. L. E. Castillo-Meza, C. A. Cravotta, T. L. Tasker, et al., "Batch Extraction Method to Estimate Total Dissolved Solids (TDS) Release From Coal Refuse and Overburden," *Applied Geochemistry* 115 (2020): 104540.
63. S. Chen, J. Xie, and Z. Wen, "Microalgae-Based Wastewater Treatment and Utilization of Microalgae Biomass," *Advanced Bioenergy* 6 (2021): 165–198.
64. P. Sudarshan, M. K. Mahesh, and T. Ramachandra, "V Assessment of Seasonal Variation in Water Quality and Water Quality Index (WQI) of Hebbal Lake, Bangalore, India," *Environmental Ecology* 37 (2019): 309–317.
65. Z. Yousefi, R. A. Mohammadpour Tahmtan, and F. Kazemi, "Temporal and Spatial Variation of Hardness and Total Dissolved Solids Concentration in Drinking Water Resources of Ilam City Using Geographic Information System," *Environmental Health Engineering And Management Journal* 2 (2015): 203–209.
66. N. H. Omer, "Water Quality Parameters," *Water Quality Assessments Policy* 18 (2019): 1–34.
67. M. M. Rahman, T. Haque, A. Mahmud, et al., "Drinking Water Quality Assessment Based on Index Values Incorporating WHO Guidelines and Bangladesh Standards," *Physics and Chemistry of the Earth Parts A/B/C* 129 (2023): 103353.
68. S. S. Khan, H. Tareen, U. Jabeen, et al., "Quality Assessment of Drinking Water From the Different Colonies of Quetta City, Pakistan According to WHO Standards," in *Proceedings of the Biological Forum, Research Trend* (2015), 699.
69. H. Ngabirano, D. Byamugisha, and E. Ntambi. Effects of seasonal variations in physical parameters on quality of gravity flow water in Kyanamira Sub-County, Kabale District, Uganda. (2016).
70. I. Narin, M. Soylak, K. Kayakirilmaz, L. Elci, and M. Dogan, "Speciation of Cr (III) and Cr (VI) in Tannery Wastewater and Sediment Samples on Ambersorb 563 Resin," *Analytical Letters* 35 (2002): 1437–1452.
71. L. Elçi, Ü. Divrikli, and M. Soylak, "Inorganic Arsenic Speciation in Various Water Samples With GFAAS Using Coprecipitation," *International Journal of Environmental Analytical Chemistry* 88 (2008): 711–723.

## Supporting Information

Additional supporting information can be found online in the Supporting Information section.